Energy materials

CrossMark

Highly porous nitrogen-doped seaweed carbon for high-performance lithium–sulfur batteries

Luke Hencz[1], Xingxing Gu[1,2,*], Xiaosong Zhou[1], Wayde Martens[3], and Shanqing Zhang[1,*]

[1] Center for Clean Environment and Energy, Environmental Futures Research Institute, Griffith School of Environment, Griffith University, Gold Coast Campus, Southport, QLD 4222, Australia
[2] College of Environment and Resources, Chongqing Technology and Business University, Chongqing 400067, China
[3] Science and Engineering Faculty, Queensland University of Technology, Brisbane, QLD 4001, Australia

ABSTRACT

Due to its natural abundance, low cost and environmental sustainability, carbon derived from biomass has been widely utilized for energy storage and conversion. Herein, we report a facile strategy to synthesize a hierarchically porous carbon via the pyrolysis of seaweed biomass under inert atmosphere and apply it as a cathode material in lithium–sulfur (Li-S) batteries for the first time. Systematic materials characterization suggests that the seaweed carbon (SWC) is doped with N and displays micro-, meso- and macroporous structures and possesses a high total pore volume of 1.48 cm^3 g^{-1} and a high surface area of 1510.71 m^2 g^{-1}, which is beneficial for encapsulating a large amount of sulfur. The as-obtained SWC-S composite, containing 65.7 wt% sulfur content, delivered a high initial discharge capacity of 1221.2 mAh g^{-1} and retained a capacity of 826.4 mAh g^{-1} after 70 cycles at 0.2 C. Additionally, the SWC-S composite produced a reversible capacity of 540.6 mAh g^{-1} after 300 cycles at high rate of 1 C. Compared to the pure sulfur cathode, the SWC-S cathode displays excellent rate capabilities, low polarization and good reaction kinetics, highlighting that this biomass-derived porous carbon is suitable for assembling high-performance Li-S batteries.

Introduction

Biomass plays an important role in humanities quest to minimize the effects of our technological advances on the environment through the use of more sustainable and environmentally benign materials. Along with the inherent characteristics of being environmentally friendly, biomass-derived carbons are reproducible, scalable, cheap and highly versatile [1]. They have been employed to combat climate change through carbon sequestration [2], improve soil quality as an ameliorant [3] and adsorb heavy metals and organics in wastewater [4, 5]. What is more, they have recently been receiving increased attention for energy storage applications [6, 7].

Address correspondence to E-mail: xingxing.gu@griffithuni.edu.au; s.zhang@griffith.edu.au

Seaweed is an attractive biomass precursor, as it is environmentally friendly, low cost, and has a wide range of applications. The global annual production of seaweed now exceeds 19 million tonnes [3], 8 million tonnes of which is from aquaculture [8], highlighting its accessibility. Seaweed carbon is an effective soil ameliorant, due in part to its trace element content (N, P and K) [3], and has also been found useful in energy-related applications, such as lithium ion batteries [9, 10], fuel cells [11, 12] and super capacitors [13, 14]. This success can be ascribed to its unique morphology, derived from its organic structure, wherein its cell walls are primarily composed of fibrous cellulose networks and alginate mucilage [11]. During growth, the alginate polymers can cross-link with metal cations (i.e., Ca^{2+}, Mg^{2+} Fe^{3+}) in the water, to form metal alginates (M-alginates) [11, 13]. Carbonization of the M-alginates carried out in inert gases environments, followed by the removal of these cations via acid washing, is expected to produce an abundant hierarchical porous seaweed carbon [13].

Hierarchical porous carbon has been successfully employed for encapsulating sulfur in the assembly of high-performance lithium–sulfur (Li-S) batteries [15–19]. Li-S batteries, with their high theoretical specific capacity (1672 mAh g^{-1}) and theoretical specific energy density (2600 Wh kg^{-1}) [20], are a promising alternative to current generation Li ion batteries that are approaching their theoretical capacity ($\approx 274/\approx 170$ mAh g^{-1} for $LiCoO_2$/ $LiFePO_4$, respectively) [20] but are insufficient for large-scale energy storage and long-range electric vehicles [15–18]. However, the commercialization of Li-S batteries is hindered by the insulating nature of sulfur [21], severe polysulfide shuttling [20, 22] and significant volume expansion at the electrode [23]. It is well established that hierarchical porous carbonaceous nanomaterials, especially N-doped carbonaceous materials, have suitable conductivity to overcome sulfur's insulating characteristics, while the abundant pores address the issues arising from the polysulfide shutting phenomenon through sulfur entrapment in the micropores/mesopores as well as accommodating the electroactive material's volume expansion. In the past decade, although high-cost carbon nanotubes (CNTs), carbon nanofibers (CNFs) and graphene have been intensively used to overcome the barriers, only limited progress has been achieved [16, 17, 24]. Therefore, hierarchical porous carbon fabricated from biomass has been receiving increased attention, as they often naturally possess rich micro- and nanostructures, which are highly desirable properties for a sulfur host in Li-S cells [25, 26].

In this work, we synthesize a hierarchical porous and nitrogen-doped seaweed carbon for Li-S batteries (as shown in Scheme 1). The as-fabricated material is subject to extensive physical and electrochemical characterization in order to illustrate a mechanism for the SWC-S composite's excellent cycling stability and rate capabilities. Additionally, selecting seaweed as the precursor to prepare porous carbon not only can reduce preparation costs through low-cost precursors; mass production could easily be achieved through scalable reaction steps to assemble high-performance carbon-S composites cathodes in bulk.
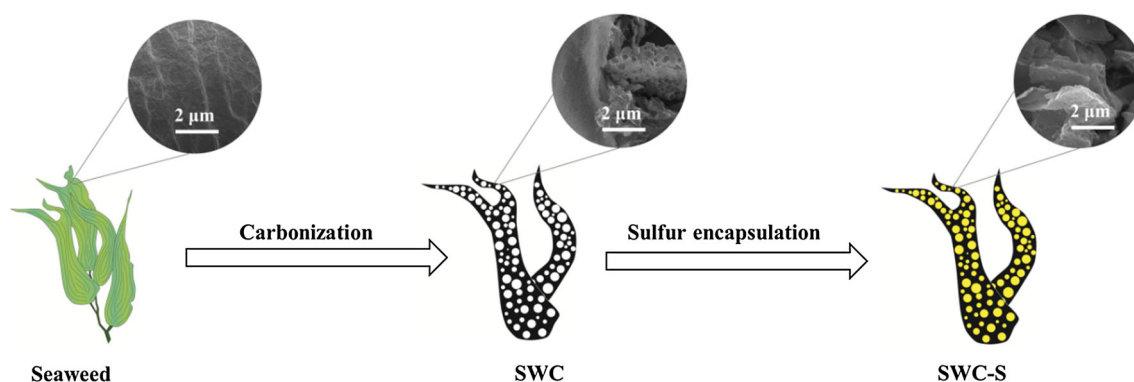
Scheme 1 Synthesis of the seaweed carbon (SWC) via carbonization (**a**) and the formation of the SWC-S composite via a thermal injection of sulfur process (**b**).

Figure 1 SEM images of SWC (**a**) and SWC-S (**b**); TEM images of SWC (**c**) and SWC-S (**d**); and HR-TEM images of SWC (**e**) and SWC-S (**f**).
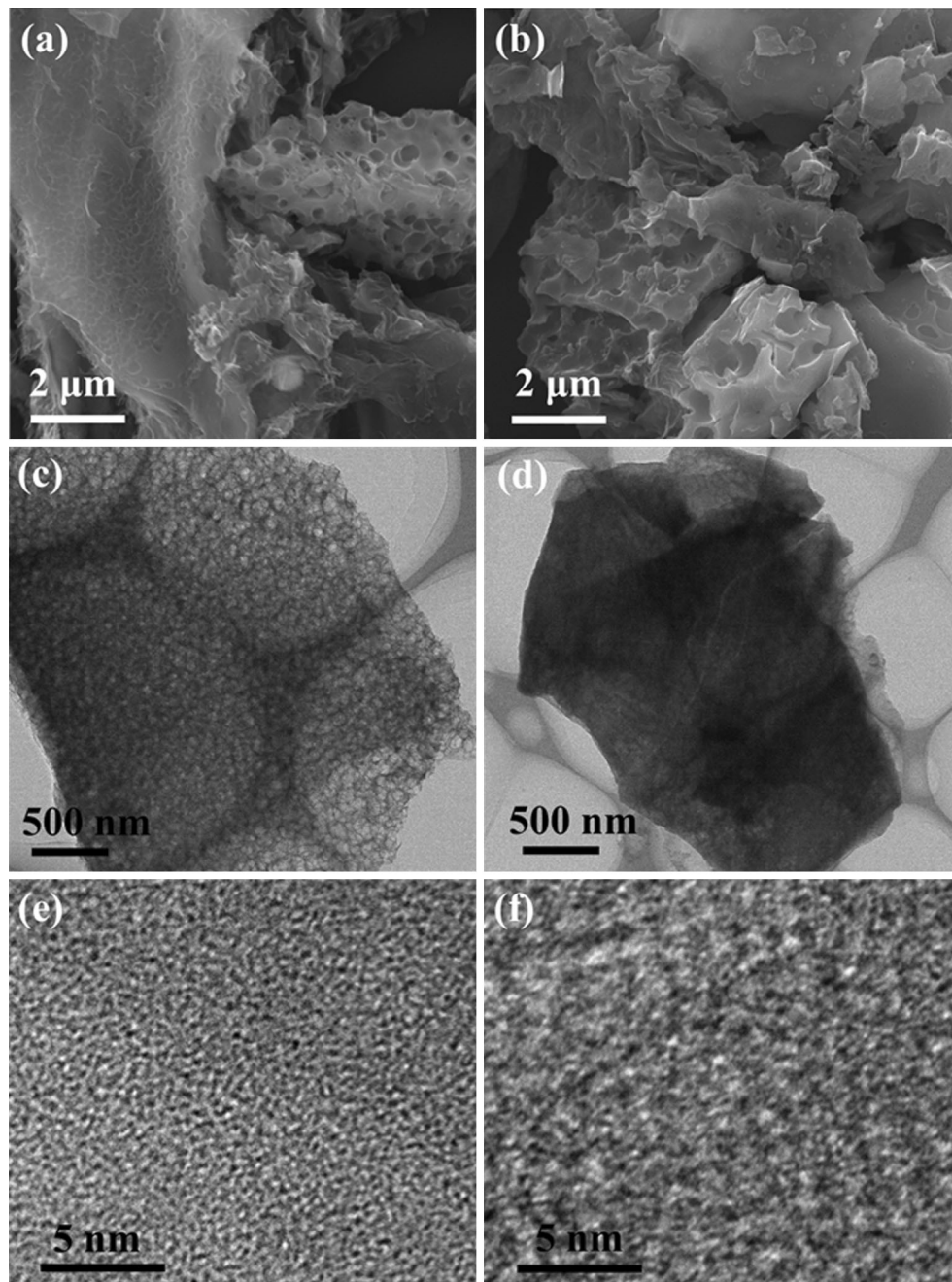

Materials and methods

Materials preparation

Seaweed carbon (SWC) preparation

First, the brown seaweed, collected from Gold Coast, Australia, was cleaned and dried at 80 °C in air for 10 h in an oven. Two grams of the dried seaweed was added into a 100-ml saturated NaCl (analytical reagent, Sigma-Aldrich) solution and stirred for 4 h. Following this, the solution was vacuum filtered and the obtained NaCl-treated seaweed was freeze-dried for 24 h, followed by thorough grinding in a mortar and pestle to disperse the NaCl porogen throughout the dried seaweed. The dried seaweed/NaCl porogen was annealed in a tube furnace at 800 °C for 2 h under an Ar atmosphere for a one-step carbonization and activation process. After cooling to room temperature, the obtained black powder was sonicated in
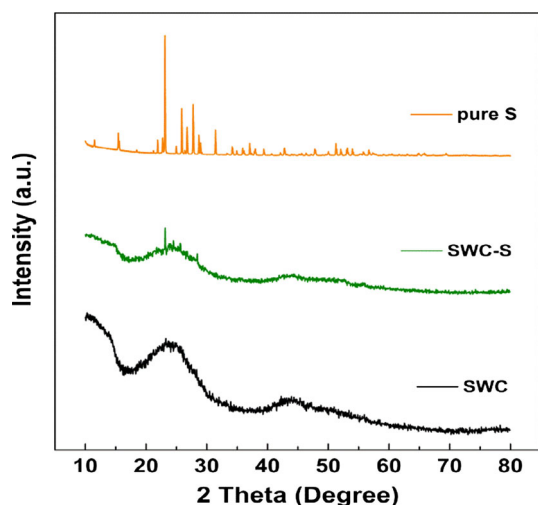
Figure 2 XRD patterns of pure sulfur, SWC, SWC-S samples.
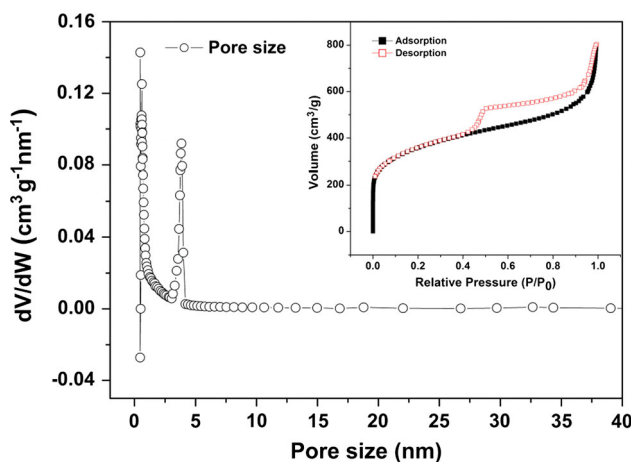
Figure 3 N$_2$ adsorption/desorption isotherms (*inset*) with the corresponding pore size distribution for SWC.

1 M HCl (analytical reagent, Univar) solution for 1 h. Following this, the solution was vacuum filtered and washed with distilled water, until a neutral pH was obtained, and ethanol in order to remove any salts, coal tar, etc. The SWC sample was subsequently obtained after vacuum drying at 60 °C overnight.

Seaweed carbon–sulfur (SWC-S) composites preparation

0.70 g sulfur was mixed with 0.30 g dry SWC thoroughly by grinding in a mortar and pestle. Then, this mixture was transferred into a sealed Teflon container and heated to 155 °C for 12 h to force the sulfur into the porous structure via the standard melt-diffusion approach [17–20]. Following this, the SWC-S composite was subjected to a 300 °C heat treatment

for a further 1 h to remove any free sulfur on the surface of the SWC. All the heating processes were carried out in an Ar atmosphere.

Materials characterization

The cleaned seaweed and SWC samples were digested in accordance with EPA 3052 methods using a Mars 6 microwave (CEM, USA). Metal ion concentrations (Fe^{3+}, Ca^{2+} and Mg^{2+}) in both the cleaned seaweed and SWC samples were determined via inductively coupled plasma optical emission spectroscopy (ICP-OES), carried out on an ICP-OES 720 series (Agilent, USA) with an axial torch. X-ray diffraction (XRD) patterns were conducted in a Model LabX-6000 diffractometer (Shimadzu, Japan) using Cu Kα radiation ($\lambda = 1.54$ Å) at 40 kV and 40 mA between the 2θ range of 10–80°. The specific surface areas and pore volumes of SWC and SWC-S composites were measured by N$_2$ adsorption/desorption at 77 K on a Tristar 3000 system (Micromeritics, USA). Pore size distribution plot was obtained by the Horvath–Kawazoe method from the adsorption branch of the N$_2$ adsorption/desorption isotherms. Thermogravimetric analyses (TGA) were carried out under an N$_2$ atmosphere from room temperature to 600 °C with an increasing rate of 10 °C min^{-1} on a series Q500 instrument (TA Instruments, USA) to determine the accurate sulfur loadings in the SWC-S composites. X-ray photoelectron spectroscopy (XPS) measurements were taken on an Axis Ultra (Kratos Analytical Ltd.) imaging photoelectron spectrometer using a monochromatized Al Kα anode, and the C 1 s peak at 284.8 eV was taken as an internal standard. The microstructure and morphology of all samples were examined using a JSM-7001F scanning electron microscope (SEM) (JEOL, Japan) and a Model Tecnai 20 transmission electron microscope (TEM) (FEI, USA) with an acceleration voltage of 200 kV. High-resolution transmission electron microscopy (HR-TEM) analyses were performed using an FEI Tecnai F30 microscope (Philips-FEI, Netherlands) operating at 300 kV.

Electrode fabrication and characterization

The as-prepared SWC-S composite were mixed with carbon black and polyvinylidene fluoride (PVDF, analytical reagent, Sigma-Aldrich) in a weight ratio of 80:10:10 with 1-methyl-2-pyrrolidinone (analytical
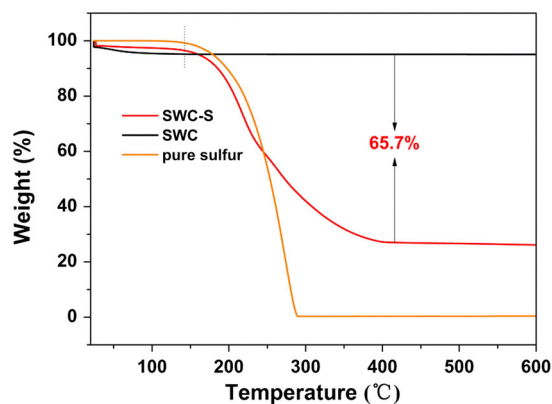
Figure 4 TGA profiles of pure sulfur, SWC and SWC-S samples.
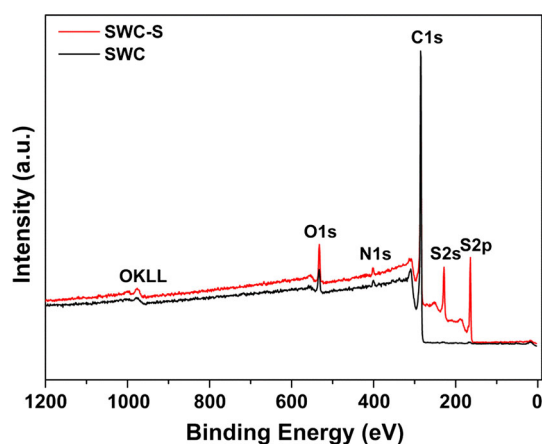
Figure 5 XPS survey spectra of the SWC and SWC-S samples.

reagent, Sigma-Aldrich) as the solvent. For comparison, pure S cathodes were fabricated using a mixture of sulfur, carbon black and PVDF in a weight ratio of 53:37:10 with 1-methyl-2-pyrrolidinone as the solvent. After stirring for 12 h, the obtained slurry was pasted on the aluminum foil via the blade-coating method, followed by drying at 60 °C in a vacuum oven for 12 h. Then, the electrode wafers were obtained by using a hole-punch to cut 0.5 cm^2 disks to form the working electrode, with an average weight of approximately 2.0 mg. The half-cells were assembled in a 2032 coin cell module in a glove box (MBRAUN, USA) under a high-purity argon atmosphere. The configuration consists of the as-fabricated working electrode (SWC-S and pure S, respectively) lithium metal as both the counter and reference electrode, polypropylene (Celgard 2300) as the separator and 1 M lithium bis(trifluoromethane)sulfonimide (LiTFSI) in 1,3-dioxolane/1,2-dimethoxyethane

(DOL/DME) (1:1, v/v) containing 0.2 M LiNO$_3$ as the electrolyte. The calculation of the specific capacity is based on the mass of the sulfur active material.

The charge and discharge performances of the half-cells were tested with a LAND CT-2001A instrument (Wuhan, China), and the potential range was controlled between 1.5 and 3.0 V at room temperature. A CHI 660D electrochemical workstation (CHI Instrument, Shanghai, China) was used to perform the CV measurements with a scan rate of 0.1 mV s^{-1} and a potential from 1.5 to 3 V. Electrochemical impedance spectroscopy (EIS) was also recorded using the same instrument over the frequency range from 100 kHz to 10 mHz.

Results and discussion

The surface of the received seaweed contained sand and other contaminants, so before drying the seaweed was washed in distilled water. After oven drying in air for 10 h, the soft, green–brown seaweed became hardened and dark brown, and lost approximately 95 wt% of water. Then, after stirring in a NaCl solution for another 12 h, the NaCl-treated seaweed was freeze-dried, which removed any remaining water. Therefore, among the remaining plant matter, the freeze-dried seaweed's cell walls contained alginate polymers and cross-linked metal cations that were present in the salt water growth medium [13, 27, 28]. It is reported that the carbonization of seaweed biomass at high temperature under inert atmospheres, followed by the removal of these metal cations from the cell wall structure via acid washing, will result in a highly porous carbon material [13]. The ICP analysis revealed the content of the Fe^{3+}, Ca^{2+} and Mg^{2+} ions in the fresh seaweed is 0.062, 12.929, 6.481 mg g^{-1}, respectively, whereas these ions content in the SWC samples is drastically reduced to 0.003, 0.021 and 0.035 mg g^{-1} for Fe^{3+}, Ca^{2+} and Mg^{2+}, respectively (Table S1). This preliminary test indicates the cross-linked ions were successfully removed by the acid washing process after carbonization.

In order to confirm the desired morphology was obtained, the SWC was subject to SEM and TEM characterizations. Abundant macropores are visible when observed under SEM (Fig. 1a), with plenty of micro-/mesopores being present under TEM and HR-TEM observation (Fig. 1c, e, respectively). In
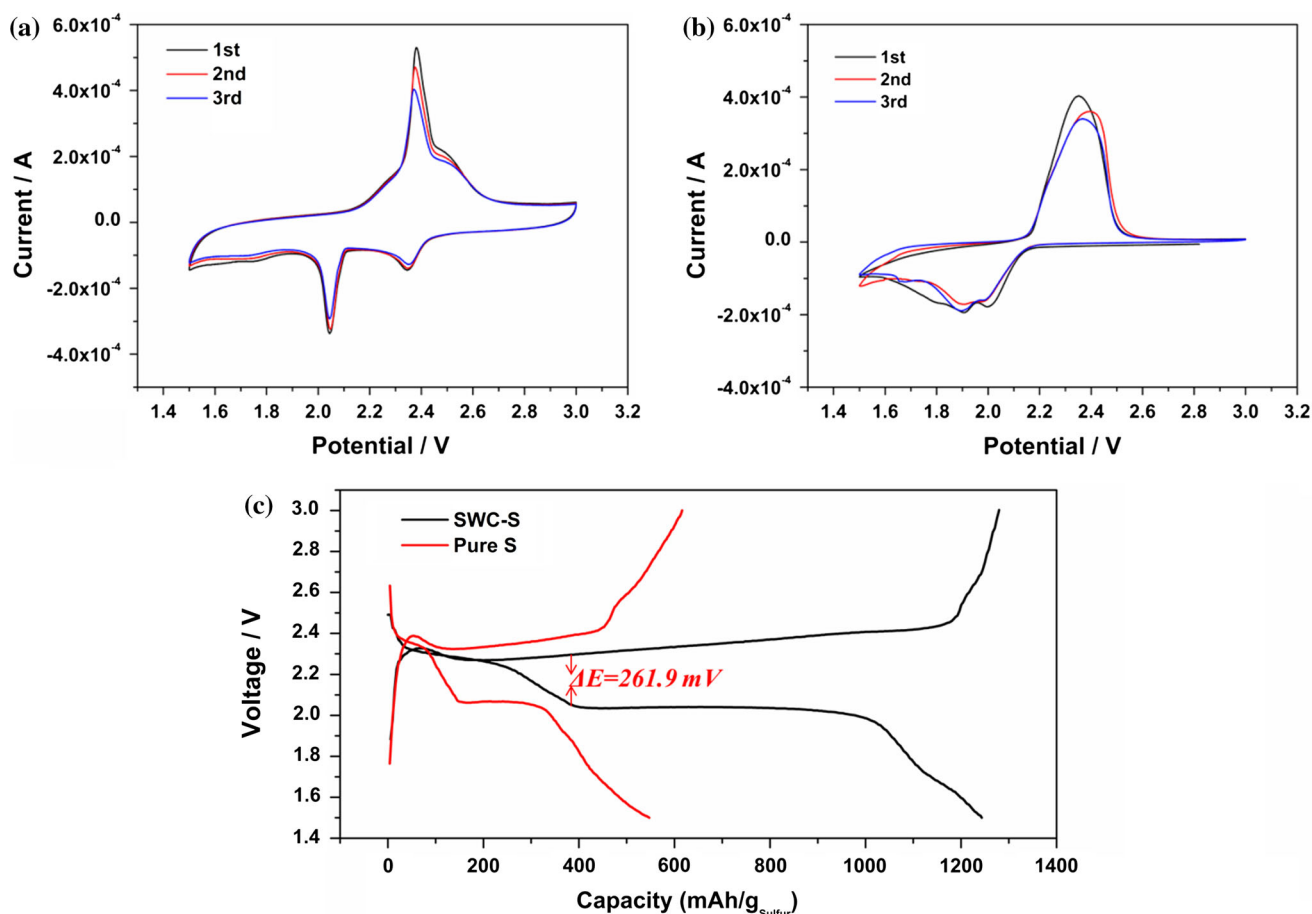
Figure 6 CVs of the SWC-S (**a**) and pure S (**b**) cathodes at a scan rate of 0.1 mV s^{-1} in the voltage range of 1.5–3.0 V versus Li$^+$/Li; Galvanostatic first charge–discharge cures of the SWC-S and pure S cathodes (**c**) at a current rate of 0.2 C tested in the voltage range of 1.5–3.0 V versus Li$^+$/Li.

contrast, the cleaned seaweed does not have pores, as shown in Fig S1; therefore, the likely mechanism for the formation of the porous structure of the SWC is the carbonization at high temperature followed by the acid wash, which successfully removed the metal cations, and the removal of the NaCl porogen. Such a hierarchical pore structure facilitates electrolyte infiltration, provides benefits by trapping the active materials and also accommodates the severe volume expansion during the discharge processes [25, 26]. Additionally, morphological investigation of the SWC-S composite was carried out. On a larger scale, SEM imaging was employed to ensure that a homogenous distribution of sulfur with no agglomeration on the surface was obtained, as displayed in Fig. 1b. This suggests the 300 °C heat treatment removed excess sulfur on the surface. On a smaller scale, TEM imaging was employed to confirm that the 155 °C heat treatment trapped the sulfur into the

micro-/mesopores and the 300 °C heat treatment for 1 h did not remove the sulfur entirely, as evidenced by the absence of vacant pores in Fig. 1d and f. The fact that the sulfur was successfully incorporated into the porous structure of the SWC was further justified by XRD analysis. As shown in Fig. 2, it can be observed the SWC displayed two broad diffraction peaks at 2θ angle of around 25° and 45°, which suggests that the obtained SWC consists of amorphous carbon and did not undergo complete graphitization [7]. After the SWC-S underwent the two subsequent heating processes (155 and 300 °C), the characteristic diffraction peaks associated with the sulfur almost disappears completely, further suggesting the sulfur is predominantly trapped in the pores of SWC rather than dispersed on the surface of the SWC [25].

To further confirm the hierarchical pore structure of the SWC and the sulfur encapsulation of the SWC-S, N$_2$ adsorption/desorption tests were conducted. The SWC
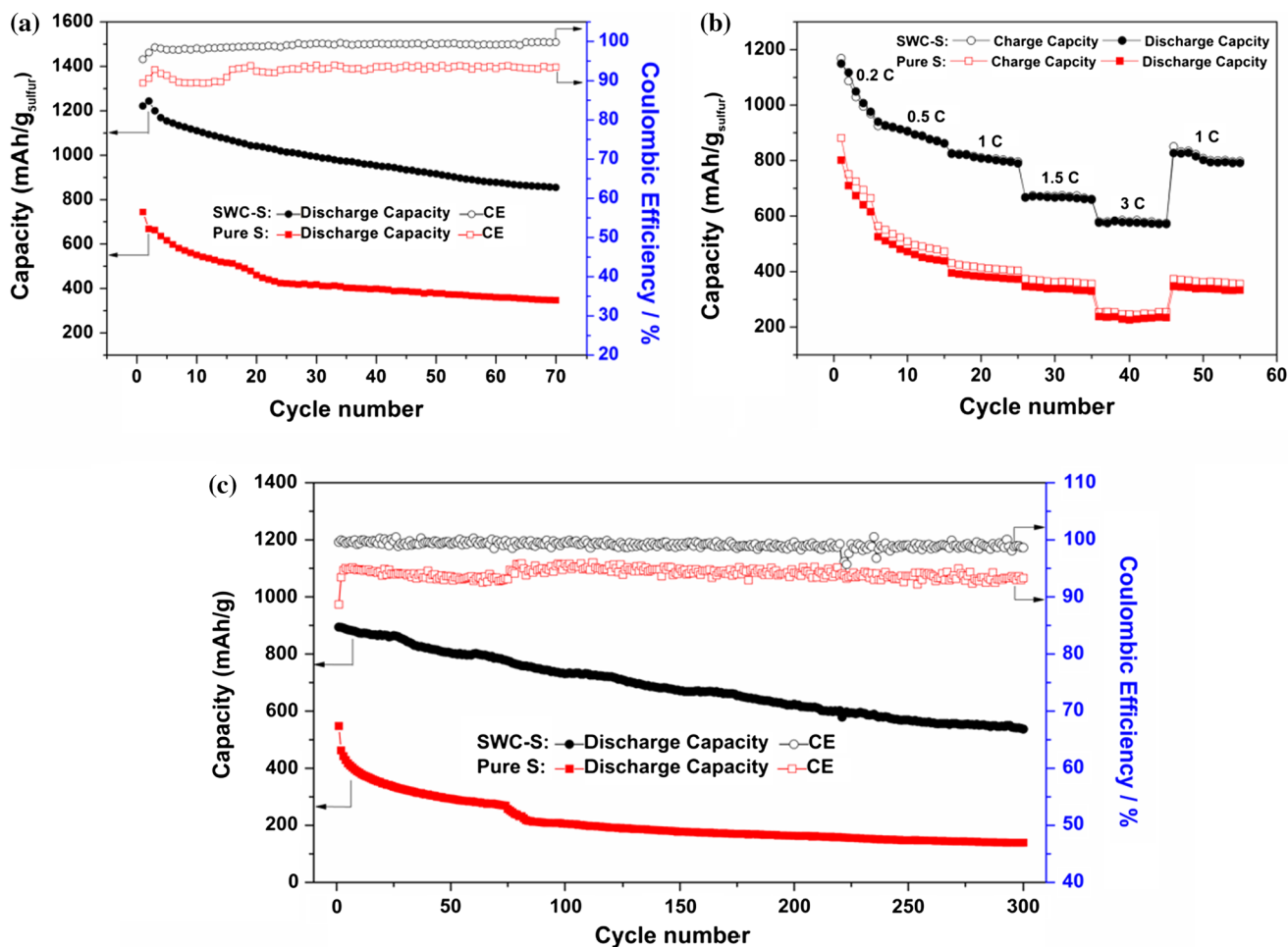
Figure 7 (**a**) Cyclic performance and coulombic efficiency of SWC-S and pure S cathodes for 70 cycles at current rate of 0.2 C in the voltage range of 1.5–3.0 V versus Li$^+$/Li; (**b**) the rate capability of SWC-S and pure S cathodes in the voltage range of 1.5–3.0 V versus Li$^+$/Li; (**c**) the long-term cycling performance and coulombic efficiency of the SWC-S electrode at the current rate of 1 C in the voltage range of 1.5–3.0 V versus Li$^+$/Li.

shows the combination of type I and IV isotherms curves, indicating abundant micropores and mesopores present in the SWC [19] (Fig. 3 inset). The pore size distributions (Fig. 3) also prove the existence of micropores ($\approx$0–1 nm) and mesopores ($\approx$4 nm), agreeing well with the SEM and TEM results. In addition, the BET surface areas and pore volumes of SWC reach as high as 1510.71 m^2 g^{-1} and 1.48 cm^3 g^{-1}, whereas the SWC-S composites illustrate extremely low BET surface areas and pore volumes of 38.64 m^2 g^{-1} and 0.035 cm^3 g^{-1}, respectively (Table S2). These results suggest the sulfur is adsorbed firmly within the internal structure of the SWC, as there is no visible agglomeration on the surface (Fig. 1b), and implies the SWC-S material is a composite.

In order to determine precisely how much sulfur was loaded within the porous structure, the SWC and SWC-S were subject to TGA. Investigation of the SWC-S composite revealed the weight percentage of sulfur was 65.7% (Fig. 4). Considering sulfur content has only reduced by approximately 5% from its initial mixture ratio (70 wt%), it is implied that the majority of the active materials are extensively confined within the SWCs pores. Further evidence of this adsorption is obtained by examining the TGA profile for pure sulfur, which evaporates completely at 300 °C, and comparing it with the temperature of complete evaporation of sulfur in the SWC-S composite (400 °C). Additionally, the TGA profile for SWC remains unchanged up to 600 °C, suggesting the structure is maintained.

Due to the fact the biomass commonly contains nitrogen atoms (in the form of proteins, amino acids, etc.), the carbonized biomass is usually self-doped
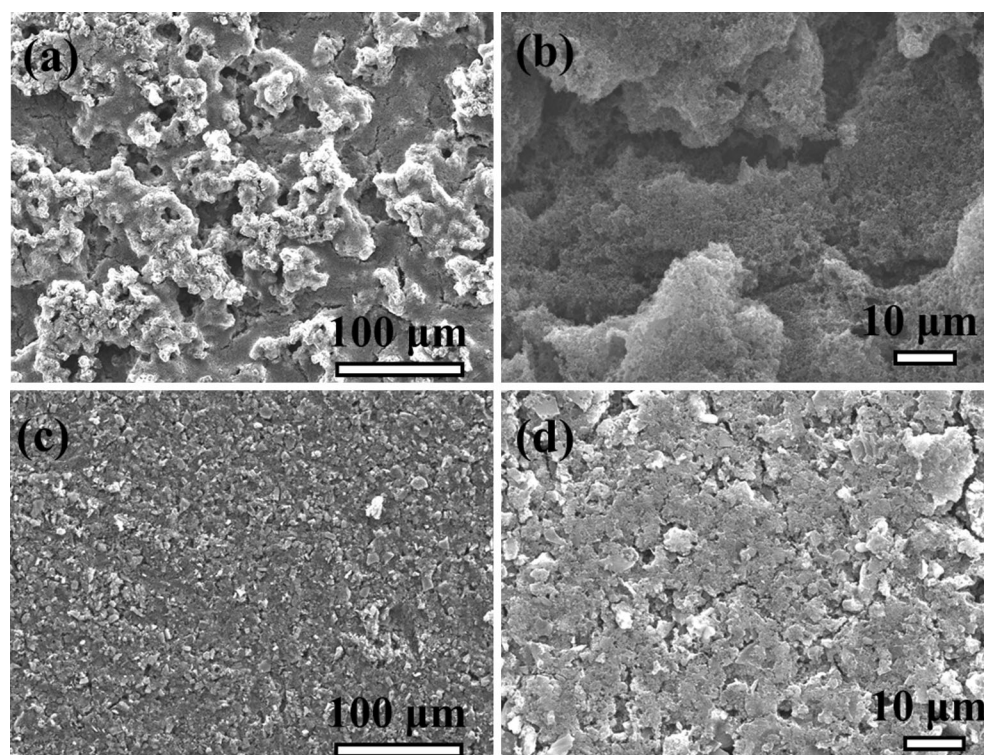
Figure 8 SEM images of the pure S cathode before cycling (**a**) and after 100 cycles (**b**) and SEM images of the SWC-S cathode before cycling (**c**) and after 100 cycles (**d**) at the current of 1 C in the voltage range of 1.5–3.0 V versus Li$^+$/Li.

with nitrogen heteroatoms during the annealing process [3]. XPS characterization was used to examine the types and contents of elements in the SWC and SWC-S samples. In addition to the expected presence of elements C and O in the SWC sample, there is also nitrogen present with a content of 2.23% in the SWC samples (Fig. 5). The presence of nitrogen within the carbon structure, which has been shown to enhance conductivity of the carbon host as well as increase the adsorption ability of the active materials, gives another potential benefit for this material when used in Li-S batteries [29]. Additionally, the characteristic S peaks can be observed in the XPS spectrum of the SWC-S, but the content is only 7.96% (Table S3), which is far lower than the content of sulfur in the SWC-S determined via TGA. That is because nearly all the sulfur flowed into the empty pores during the heating process rather than simply being dispersed on the surface of the SWC.

In order to investigate the electrochemical performances of the fabricated composite, a Li-S battery was assembled with the SWC-S composite immobilized on carbon-coated aluminum foil as a cathode and a pure lithium metal as an anode. The CV curves of the first three cycles have been obtained to investigate electrochemical mechanisms of the Li-S battery. Two reduction peaks at 2.30 and 2.05 V are present (Fig. 6a), which typically correspond to the reduction in S_8 to high-order polysulfides Li_2S_x ($4 \leq x \leq 8$) and low-order polysulfides (Li_2S_2 and Li_2S), respectively [25, 30]. The oxidation peak at 2.35 V could be attributed to the transformation of Li_2S_2 and Li_2S into high-order polysulfides Li_2S_x ($4 \leq x \leq 8$). The shoulder may correspond to the further oxidation of high-order polysulfides Li_2S_x ($4 \leq x \leq 8$) to S_8 [25, 30]. Compared with the CV curves of the pure S cathode (Fig. 6b), even though it also illustrates two reduction peaks, the peak positions have shifted to the lower voltage of 2.05 and 1.9 V, respectively; the peak shapes become broader and the peak currents decrease, all of which demonstrate the more serious polarization of the pure S cathode and consequently better stability of the SWC-S cathode [25]. What is more, the typical charge/discharge voltage profiles further prove the superiority of the SWC-S cathode. Figure 6c shows the initial galvanostatic charge/discharge voltage profiles of pure S and SWC-S cathodes. It is clearly observed that the SWC-S cathode illustrates two discharge plateaus, corresponding well with the CV
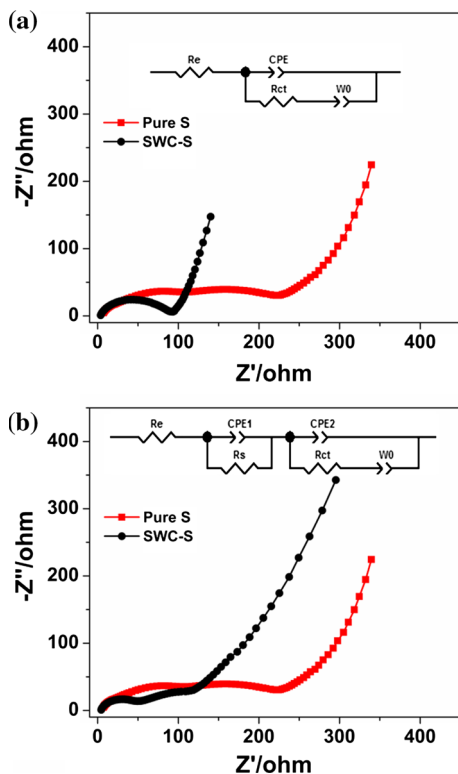
Figure 9 Nyquist plots before first discharge (**a**) and after the 100th discharge (**b**) for pure S cathode and SWC-S cathodes.

Table 1 Impedance parameters simulated from the equivalent circuits

Cycle number	Sample	Resistance (Ω)		
		R_e	R_s	R_{ct}
Before cycling	SWC-S	1.6	–	88.8
	Pure S	3.5	–	204.7
After 100 cycles	SWC-S	4.5	5.9	70.8
	Pure S	3.9	39.6	103

curves. However, due to the severe self-discharge, the first and second reduction peaks are severely reduced for the pure S cathode. Furthermore, the voltage gap (ΔE) of SWC-S is much smaller than that of pure S cathode (261.9 *vs.* 414.3 mV), which also indicates the lower polarization and high stability of the SWC-S electrode [22]. In summary, both the CV curves and charge/discharge voltage profiles suggest the SWC host effectively improves the electrochemical behaviors of the electrodes, which is ascribed to the carbon skeleton improving conductivity, with abundant pores and doped N atoms inhibiting the polysulfide shuttle [31].

The cyclability of the SWC-S and pure S cathodes is compared in Fig. 7a. The SWC-S cathode shows an initial capacity of 1221.2 mAh g^{-1} at 0.2 C, which is 73% of its theoretical capacity (1675 mAh g^{-1}) and almost 1.6 times higher than the pure S electrode (only 756.3 mAh g^{-1}). After 70 deep charge/discharge cycles, a reversible discharge capacity of 855.0 mAh g^{-1} is obtained, while the pure S cathode decreases quickly to 346.4 mAh g^{-1}. Therefore, it is obvious that the SWC-S cathode demonstrates higher sulfur utilization and better capacity retention than that of the pure S electrode. In addition, the SWC-S cathode reveals better coulombic efficiency (CE) for 70 cycles, at around 99% compared to the pure S cathode with only about 94%. The rate capabilities of SWC-S cathode and pure S cathode are shown in Fig. 7b. For the SWC-S cathode, a highly reversible capacity of 826.4 mAh g^{-1} is obtained at 1 C; when the current increases to 3 C, a capacity of 576.4 mAh g^{-1} still can be achieved. Following on when the C rate switches back to 1 C, the capacity recovers to approximately 800 mAh g^{-1}, suggesting excellent electrode integrity and fast reaction kinetics in the SWC-S electrode [32]. In contrast, the pure S cathode shows an extremely weak capability at the high C rate and could not recover to its original capacity when switching back to the lower charge/discharge C rate.

Additionally, the SWC-S and the pure S cathodes were subjected to long-term cycling investigation as shown in Fig. 7c. The pure S cathode shows an initial capacity of only 547.8 mAh g^{-1} followed by a sharp decrease. After 300 cycles, a radically low capacity of 139.1 mAh g^{-1} was retained. However, the SWC-S cathode delivers an initial capacity of 893.5 mAh g^{-1}, 53.3% of its theoretical capacity, at a high charge/discharge current. After 300 cycles, the capacity stabilizes at 540.6 mAh g^{-1} with a high CE of around 98% and displays a low capacity decay of only 0.13% per cycle, which is superior to most of the biochar-S, nitrogen-doped graphene-S, CNF-S and CNT-S composites as shown in Table S4. These results indicate the excellent stability of SWC-S cathodes, which could be attributed to SWC host responsible for the effective inhibition of the polysulfide shuttle effect.

Since the SWC-S cathode exhibits far better electrochemical performances compared to the pure S cathode, it is highly likely the success of the SWC as the sulfur host stems from its ability to maintain

electrode integrity, improve the conductivity and confine polysulfides within the cathode. Therefore, the physical and electrochemical properties of SWC-S cathode are systematically investigated to explore possible mechanisms responsible for the improvement in cycling performance. The SEM images of the pure S cathode and SWC-S cathode before and after cycling are employed to investigate the integrity of the electrode. As shown in Fig. 8, it is obvious the SWC-S cathode (Fig. 8c) illustrates better homogeneity compared to the pure S cathode (Fig. 8a) before cycling. Primarily when the sulfur content is too high to be adequately confined within a conductive matrix, it can easily aggregate, which results in the inhomogeneity displayed by the pure S electrode. However, when the sulfur is encapsulated into the SWC, this phenomenon has been essentially eliminated. After being subjected to 100 charge/discharge cycles, the SWC-S electrode (Fig. 8d) still exhibits relative structural integrity, while the pure S electrode (Fig. 8b) demonstrates severe cracks and large pores, which both imply the electrode integrity has been compromised [16].

In order to further explore the mechanism of the enhanced electrochemical performances of the SWC-S, EIS measurements before cycling and after 100 cycles were taken. The EIS data in Fig. 9a show the impedance before discharging. The Nyquist plots consist of a depressed semicircle in the high-frequency region and an oblique line in the medium-frequency region. The semicircle is attributed to the charge transfer resistance (R_{ct}) at the interface between the electrolyte and sulfur electrode, while the oblique line reflects the Warburg impedance (W_0) associated with the diffusion of the lithium ions into the bulk of the electrode material [33]. The high-frequency intercept on the real axis represents the ohmic resistance (R_e) of the cell, which includes the electrolyte and electrode resistances [34]. Figure 9b reveals the impedance after 100 cycles, where the Nyquist plots are made up of two semicircles and a sloping line. The semicircle in the higher frequency region reflects the interfacial charge transfer resistance, and the semicircle in the medium-frequency range is related to the resistance R_s of the solid–electrolyte interface (SEI) film which is caused by the formation of Li_2S (or Li_2S_2) on the carbon matrix in the cathode [34]. It is expressly observed the semicircles of SWC-S are smaller than that of pure S cathode both before cycling and after 100 cycles. The

equivalent circuits used to calculate the fitted R_e, R_s, R_{ct} values are displayed in Fig. 9a and b, and the calculated values are given in Table 1. Before cycling, the R_{ct} value of SWC-S (88.8 Ω) is far less than that of pure S cathode (204.7 Ω), demonstrating that SWC could remarkably enhance the conductivity of the entire electrode, which is beneficial to improve reaction kinetics and active materials utilization [35]. After 100 deep discharge cycles, the R_{ct} value of SWC-S decreases slightly, due to the appropriate SEI film formation on the electrode surface facilitating the transportation of lithium ions [35]. In contrast, the R_{ct} value of pure S decreases dramatically after 100 cycles, only half of that before cycling, because large amounts of sulfur dissolved in the electrolyte, which exposed the conductive carbon black, therefore resulting in a sharp decrease in the R_{ct}. The R_s values further prove this hypothesis. As shown in Table 1, the R_s of SWC-S is only 5.9 Ω, which indicates a very thin Li_2S_2 and Li_2S film formation on the cathode surface [36], while the R_s of pure S is 39.6 Ω, 6.5 times higher than SWC-S, suggesting plentiful Li_2S_2 and Li_2S generation and a thick SEI film formation. All of the above results suggest the SWC effectively inhibits the sulfur from dissolving in the electrolyte by physical and chemical adsorption, and thus, the SWC-S exhibits enhanced electrochemical performances in comparison with the pure S cathode.

Conclusion

Seaweed is a commercially available, cheap and environmentally friendly material that was used to synthesize the hierarchical porous and nitrogen-doped carbon material. When the prepared seaweed carbon was employed in Li-S batteries, the as-fabricated SWC-S composite demonstrates a high initial discharge capacity of 1200 mAh g^{-1} at 0.2 C and a good reversible capacity of 575 mAh g^{-1} at 1 C over 300 cycles. The prominent performances could be ascribed to the abundant porous structure and doped nitrogen atoms of SWC. The porous structure provides channels for the electrolyte to infiltrate evenly throughout the cathode materials and provides Li ion pathways for transportation which enhances the ionic conductivity. The doped N atoms, on the one hand, could further enhance the conductivity of SWC to accelerate reaction kinetics during the charge/discharge process; and on the other hand, it can

chemically bond any polysulfides to improve the cycle life of the cathode. The beneficial chemical and physical morphology, along with excellent electro-chemical performances, strongly suggests this novel SWC-S nanocomposite is a promising cathode material for Li-S batteries.

Acknowledgements

Compliance with ethical standards

Conflict of interest The authors declare no competing financial interest.

Electronic supplementary material: The online version of this article (doi:10.1007/s10853-017-1288-y) contains supplementary material, which is available to authorized users.

References

[1] Yao Y, Wu F (2015) Naturally derived nanostructured materials from biomass for rechargeable lithium/sodium batteries. Nano Energy 17:91–103

[2] Han X, Sun X, Wang C et al (2016) Mitigating methane emission from paddy soil with rice-straw biochar amendment under projected climate change. Scientific Rep 6:24731–24740

[3] Roberts DA, Paul NA, Dworjanyn SA, Bird MI, de Nys R (2015) Biochar from commercially cultivated seaweed for soil amelioration. Scientific Rep 5:9665–9670

[4] Liu RL, Liu Y, Zhou XY, Zhang ZQ, Zhang J, Dang FQ (2014) Biomass-derived highly porous functional carbon fabricated by using a free-standing template for efficient removal of methylene blue. Biores Technol 154:138–147

[5] Chen PP, Zhang HP, Luo XG, Lin XY, Lu X, Tang Y (2016) Cost effective biochar gels with super capabilities for heavy metal removal. RSC Adv 6:75430–75439

[6] Li B, Geng D, Lee XS et al (2015) Eggplant-derived microporous carbon sheets: towards mass production of efficient bifunctional oxygen electrocatalysts at low cost for rechargeable Zn-air batteries. Chem Commun 51:8841–8844

[7] Jiang J, Zhu J, Ai W et al (2014) Evolution of disposable bamboo chopsticks into uniform carbon fibers: a smart strategy to fabricate sustainable anodes for Li-ion batteries. Energy Environ Sci 7:2670–2679

[8] Winberg PC, Skropeta D, Ullrich A (2011) Seaweed cultivation pilot trials–towards culture systems and marketable products. RIRDC 10:184, PRJ: 000162

[9] Liu L, Yang X, Lv C et al (2016) Seaweed-derived route to Fe_2O_3 hollow nanoparticles/N-doped graphene aerogels with high lithium ion storage performance. ACS Appl Mater Interfaces 8:7047–7053

[10] Lv C, Yang X, Umar A et al (2015) Architecture-controlled synthesis of M_xO_y (M = Ni, Fe, Cu) microfibres from seaweed biomass for high-performance lithium ion battery anodes. J Mater Chem A 3:22708–22715

[11] Zhao W, Yuan P, She X et al (2015) Sustainable seaweed-based one-dimensional (1D) nanofibers as high-performance electrocatalysts for fuel cells. J Mater Chem A 3:14188–14194

[12] Song MY, Park HY, Yang DS, Bhattacharjya D, Yu JS (2014) Seaweed-derived heteroatom-doped highly porous carbon as an electrocatalyst for the oxygen reduction reaction. Chemsuschem 7:1755–1763

[13] Kang D, Liu Q, Gu J, Su Y, Zhang W, Zhang D (2015) "Egg-box"-assisted fabrication of porous carbon with small mesopores for high-rate electric double layer capacitors. ACS Nano 9:11225–11233

[14] Bichat M, Raymundo-Piñero E, Béguin F (2010) High voltage supercapacitor built with seaweed carbons in neutral aqueous electrolyte. Carbon 48:4351–4361

[15] Ding B, Yuan C, Shen L, Xu G, Nie P, Zhang X (2013) Encapsulating sulfur into hierarchically ordered porous carbon as a high-performance cathode for lithium-sulfur batteries. Chem-A Eur J 19:1013–1019

[16] Liang C, Dudney NJ, Howe JY (2009) Hierarchically structured sulfur/carbon nanocomposite material for high-energy lithium battery. Chem Mater 21:4724–4730

[17] Qu Y, Zhang Z, Zhang X et al (2014) Synthesis of hierarchical porous honeycomb carbon for lithium-sulfur battery cathode with high rate capability and long cycling stability. Electrochim Acta 137:439–446

[18] Yu L, Brun N, Sakaushi K, Eckert J, Titirici MM (2013) Hydrothermal nanocasting: synthesis of hierarchically porous carbon monoliths and their application in lithium-sulfur batteries. Carbon 61:245–253

[19] Xu G, Ding B, Nie P, Shen L, Dou H, Zhang X (2013) Hierarchically porous carbon encapsulating sulfur as a superior cathode material for high performance lithium-sulfur batteries. ACS Appl Mater Interfaces 6:194–199

[20] Zhang L, Ji L, Glans P-A, Zhang Y, Zhu J, Guo J (2012) Electronic structure and chemical bonding of a graphene oxide-sulfur nanocomposite for use in superior performance lithium-sulfur cells. Phys Chem Chem Phys 14:13670–13675

[21] Zhou G, Tian H, Jin Y et al (2017) Catalytic oxidation of Li_2S on the surface of metal sulfides for Li-S batteries. Proc Natl Acad Sci 114:840–845

[22] Rehman S, Gu X, Khan K et al (2016) 3D Vertically aligned and interconnected porous carbon nanosheets as sulfur immobilizers for high performance lithium-sulfur batteries. Adv Energy Mater 6:1502518–1502525

[23] Nazar LF, Cuisinier M, Pang Q (2014) Lithium-sulfur batteries. MRS Bull 39:436–442

[24] Tang C, Zhang Q, Zhao MQ et al (2014) Nitrogen-doped aligned carbon nanotube/graphene sandwiches: facile catalytic growth on bifunctional natural catalysts and their applications as scaffolds for high-rate lithium-sulfur batteries. Adv Mater 26:6100–6105

[25] Zhang J, Xiang J, Dong Z, Liu Y, Wu Y, Xu C, Du G (2014) Biomass derived activated carbon with 3D connected architecture for rechargeable lithium-sulfur batteries. Electrochim Acta 116:146–151

[26] Yang K, Gao Q, Tan Y, Tian W, Qian W, Zhu L, Yang C (2016) Biomass-derived porous carbon with micropores and small mesopores for high-performance lithium-sulfur batteries. Chem-A Eur J 22:3239–3244

[27] Grant GT, Morris ER, Rees DA, Smith PJ, Thom D (1973) Biological interactions between polysaccharides and divalent cations: the egg-box model. FEBS Lett 32:195–198

[28] Schnepp Z (2013) Biopolymers as a flexible resource for nanochemistry. Angew Chem Int Ed 52:1096–1108

[29] Song J, Xu T, Gordin ML et al (2014) Nitrogen-doped mesoporous carbon promoted chemical adsorption of sulfur and fabrication of high-areal-capacity sulfur cathode with exceptional cycling stability for lithium-sulfur batteries. Adv Func Mater 24:1243–1250

[30] Li Z, Jiang Y, Yuan L et al (2014) A highly ordered meso@microporous carbon-supported sulfur@smaller sulfur core-shell structured cathode for Li-S batteries. ACS Nano 8:9295–9303

[31] Gu X, Lai C, Liu F, Yang W, Hou Y, Zhang S (2015) A conductive interwoven bamboo carbon fiber membrane for Li-S batteries. J Mater Chem A 3:9502–9509

[32] Li G, Ling M, Ye Y et al (2015) Acacia senegal-inspired bifunctional binder for longevity of lithium-sulfur batteries. Adv Energy Mater 5:1500878–1500885

[33] Zhao D, Qian X, Jin L et al (2016) Separator modified by Ketjen black for enhanced electrochemical performance of lithium-sulfur batteries. RSC Adv 6:13680–13685

[34] Ahn W, Kim KB, Jung KN, Shin KH, Jin CS (2012) Synthesis and electrochemical properties of a sulfur-multi walled carbon nanotubes composite as a cathode material for lithium sulfur batteries. J Power Sources 202:394–399

[35] Zhou G, Pei S, Li L et al (2014) A graphene-pure-sulfur sandwich structure for ultrafast, long-life lithium-sulfur batteries. Adv Mater 26:625–631

[36] Zhang K, Xu Y, Lu Y et al (2016) A graphene oxide-wrapped bipyramidal sulfur@polyaniline core-shell structure as a cathode for Li-S batteries with enhanced electrochemical performance. J Mater Chem A 4:6404–6410